Extended Reactive Power Exchange With Faulty Cells in Grid-Tied Cascaded H-Bridge Converter for Solar Photovoltaic Application

Rahul Sharma, *Student Member, IEEE*, and Anandarup Das, *Member, IEEE*

***Abstract*—Fault-tolerant operation is a key feature of grid-tied photovoltaic fed Cascaded H-Bridge converter, where the converter operates continuously with faulty bypassed cells. After bypassing the faulty cells, the number of healthy cells decreases, the available dc-link voltage reduces and active power among the phases become unequal. As a result, the converter produces unbalanced and distorted grid currents. Moreover, the maximum reactive power exchanged with the grid gets reduced with the available dc-link voltage. This article proposes a novel zero-sequence voltage injection technique for balancing the grid currents and preventing overmodulation in each cell of the converter. The proposed technique extends the reactive power capability of the converter during a postfault condition. Additionally, it also helps in equal active and reactive power flow in each phase of the converter. A new PWM clamping strategy is proposed in this article to implement the zero-sequence voltage addition in the converter. The proposed concept is verified through computer simulation and experimental results.**

***Index Terms*—Ancillary services, cascaded H-bridge (CHB) multilevel converters, fault tolerance, PWM clamping strategy, reactive power, solar photovoltaic (PV).**

I. Introduction

GRID-CONNECTED large scale solar photovoltaic (PV) plants are causing increased penetration of renewable energy in the grid in recent years [1], [2]. Nowadays, large scale solar PV plants not only supply active power but also exchange reactive power with the grid for ancillary services like reactive power compensation, power quality enhancement, low voltage ride through [1], [3], [23], [24], [26], etc.

Cascaded H-bridge (CHB) multilevel converter has become one of the most attractive topologies for large scale solar PV plants connected to medium voltage [3]–[5]. This topology has several benefits compared to the conventional two-level converter (PV Central Inverter) like high-quality output voltage, lower total harmonic distortion (THD), lower voltage stress on the switches, and modular structure [3]–[7]. At the medium voltage level, it can be directly connected to the grid without using a step-up line frequency transformer [7]–[9]. Due to more number of switches, the probability of switch failure is high in this converter [10]–[19], [25], [26]. The operation of the CHB converter can be improved after a fault by bypassing the faulty cells and allow the continuous operation of the converter with a reduced capacity [10], [11].

Fault tolerant operation of CHB converter has been discussed in literature for motor drives [12], [15], static volt-ampere reactive (VAR) compensations (STATCOM) [16], [18], battery energy storage system (BESS) [19], [26], and solar PV system [25].

The simplest fault method in the drive application is to bypass the faulty cell in a phase along with two healthy cells in the other two phases [12]. As a result, phase voltages and line voltages remain balanced but their magnitudes get reduced. A similar technique is also used in the STATCOM application [16]. This technique of bypassing healthy cells is not advantageous for solar PV application since active power from the converter will reduce. In [16] and [17], the dc-link voltage has to be increased to maintain converter output voltage closed to the grid voltage for supplying the rated reactive power.

The other method is to use an auxiliary two-level converter [18] or a redundant H-bridge cell in each phase of the converter [10], [11]. By using this method, the converter can be operated at the same capacity as pervious but the size and cost of the system are increased. This method is suitable for an only single faulty cell.

In other methods, after bypassing the faulty cells, the magnitude and phase of the cluster voltages are adjusted by shifting the neutral point of the converter so that the converter generates maximum possible line voltage. This method is called "fundamental frequency zero-sequence voltage injection" [12], [13], [19]. The zero-sequence voltage is used to transfer power from one phase to another to balance the currents. This method is mostly used in motor drive applications [12], [13]. The injection of zero-sequence voltage is also proposed for grid-connected CHB converter for BESS application [19] with one faulty cell. However, this method is not applicable in more than one faulty cell. The fault-tolerant method is further improved by injecting harmonics [14], [15] that provides maximum line voltage according to a fault condition and also increases the linear modulation region for motor drive application.

Several authors [7], [20]–[22] have presented different types of zero-sequence voltage injection for grid-tied solar PV

Manuscript received May 20, 2019; revised August 22, 2019; accepted October 15, 2019. Date of publication October 28, 2019; date of current version February 20, 2020. This work was supported in part by the Science and Engineering Research Board, Department of Science & Technology, Government of India under Grant SB/S3/EECE/044/2015. Recommended for publication by Associate Editor Y. Xue. *(Corresponding author: Rahul Sharma.)*

The authors are with the Department of Electrical Engineering, Indian Institute of Technology, Delhi, New Delhi 110016, India (e-mail: rahuls569@gmail.com; anandarup@iitd.ac.in).

Color versions of one or more of the figures in this article are available online at http://ieeexplore.ieee.org.

Digital Object Identifier 10.1109/TPEL.2019.2950336

application during unequal power generation among the clusters due to nonuniform irradiation, the unequal temperature of the PV cells and PV panel degradation. However, these papers have only discussed unbalanced active power generation in the cells but have not discussed the operation of CHB with faulty cells as well as reactive power exchange with the grid. The reactive power exchange with the grid has been discussed in [23] and [24] for power quality improvement during unequal power generation among the clusters with equal dc-link voltage of the cell but the three-phase grid currents are seen to be unbalanced. Moreover, these articles have not discussed the operation of CHB with bypassed faulty cells.

Yu *et al.* [25] have discussed the operation of CHB for solar PV applications with faulty cells for supplying only active power in the grid. In this article, the cluster voltage is realized by increasing the dc-link voltage of the cell to avoid over modulation. Increasing the dc-link voltage, however, puts additional voltage stress on the devices.

The primary contributions of this article are as follows.

1) A zero-sequence voltage is derived by ensuring active power supply and reactive power exchange with the grid. It helps in balancing the line voltage as well as active and reactive power exchange in the grid during a postfault condition.
2) Mathematical expression for the required dc-link voltage to prevent overmodulation is derived when the converter exchanges active and reactive power with the grid.
3) A novel PWM clamping strategy is proposed that maximizes the linear modulation region of the converter with available dc-link voltage of the cell. It helps in extending the active and reactive power exchange capability of the converter.

II. Zero-Sequence Voltage With Faulty Cells

This section describes the operation of grid-tied solar PV fed CHB converter with faulty cells. For certain active and reactive power exchanges by the converter with faulty cells, a zero-sequence voltage is derived in this section.

Fig. 1 depicts the system configuration of a grid-tied solar PV fed $(2n+1)$ level CHB converter. The system has three clusters in star configuration which is connected to the balanced grid through the filter L_f. One cluster is made of series-connected identical cells. One cell consists of solar PV, isolated dc–dc converter and H-bridge converter. A bypass switch after H-bridge converter is used to bypass the cell under fault condition.

This article assumes that active power generated among cells are equal in a cluster (i.e., $P_{a1}=P_{a2}=\cdots P_{\rm an}=P_{{\rm PV}a}$, $P_{b1}=P_{b2}=\cdots P_{\rm bn}=P_{{\rm PV}b}$ and $P_{c1}=P_{c2}=\cdots P_{\rm cn}=P_{{\rm PV}c}$, where n = number of cells in a cluster). Hence, the cumulative power in the ith phase cluster is $P_i=nP_{{\rm PV}i}\ \forall i\in\{a,b,c\}$, and the total three phase power is $P_g=P_a+P_b+P_c$. The dc-link voltage of each cell $V_{{\rm dc}ij}$ $(i\in\{a,b,c\}$, and $j\in\{1,2,\ldots,n\})$ is equal to k, and the cummulative dc-link voltage of clusters are $V_{{\rm dc}i}$ $V_{{\rm dc}i}(=V_{{\rm dc}i1}+V_{{\rm dc}i2}+,\ldots,+V_{{\rm dc\,in}}=nV_{{\rm dc}ij}=nk)$.

During one or more faults in a cell of a phase cluster, the bypass switch is activated, and it excludes the faulty cells from the converter. Now, two challenges come up: first, the active power generated among the clusters becomes unequal; and second, the cumulative dc-link voltage of the cluster becomes unequal. The cluster powers are written as

$$P_i=(n-n_i)P_{{\rm PV}i}\quad \forall i\in\{a,b,c\}. \tag{1}$$

And, the cumulative dc-link voltage of clusters is written as

$$V_{{\rm dc}i}=(n-n_i)k\quad \forall i\in\{a,b,c\} \tag{2}$$

where n_i is the number of faulty cells in ith cluster.

Since the dc-link voltages of each cluster are unequal and solar PV of each cell should operate at the maximum power point, the output ac voltages from the cluster become unbalanced and distorted. Hence, unbalanced grid currents are supplied to the grid which is not allowed by the grid codes [23]. To make the grid currents $(I_a=I_b=I_c=I_g)$ balanced, a zero-sequence voltage (V_z) is injected. V_z also ensures balanced line voltage and balanced active and reactive power is injected in the grid.

The injection of V_z during a fault in any cluster is depicted in the circuit diagram in Fig. 2. In Fig. 2, it is assumed that the grid phase voltages $(v_{\rm in}i\in\{a,b,c\})$ are balanced, and the active power and reactive power absorbed by the grid is positive $(P_g>0$ and $Q_g>0)$. The phasor diagram during this condition is shown in Fig. 3. In Fig. 3, the converter is supplying balanced currents at a power factor γ with grid voltages implying $P_g>0$ and $Q_g>0$. V_z is injected at an angle α to generate balanced line voltages (dotted black lines).

An expression of V_z is now derived. From Fig. 2, it can be seen that the interaction of V_z and the grid current I_a, I_b, and I_c generates active and reactive power. The active power produced

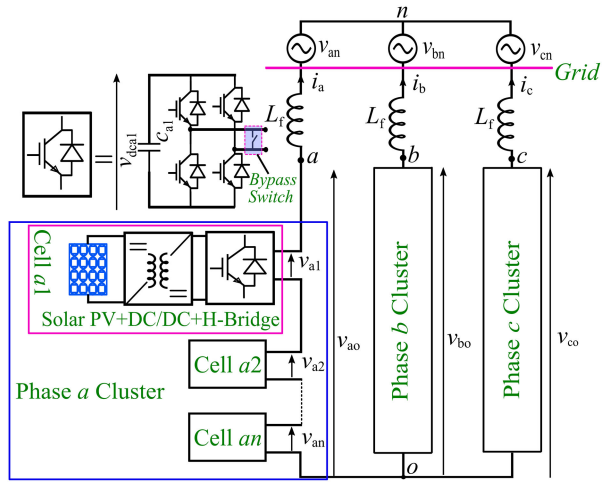

Fig. 1. Grid-tied solar PV fed CHB converter.

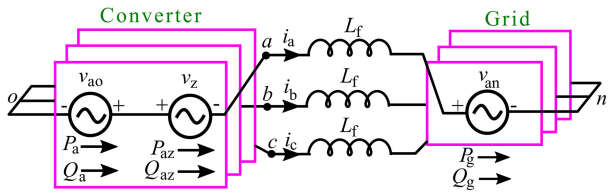

Fig. 2. Circuit diagram during the fault condition.

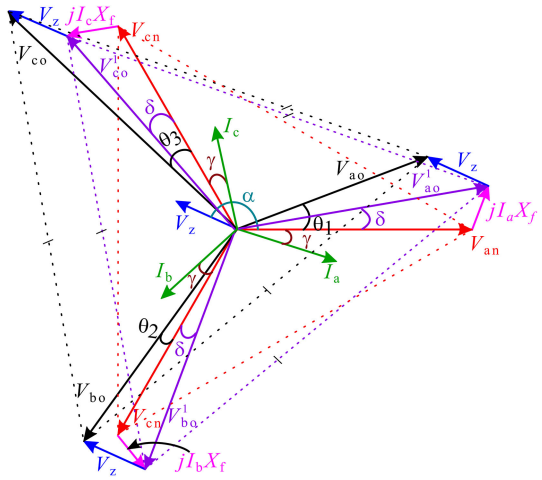

Fig. 3. Phasor diagram with faulty cell in phase a cluster.

by zero-sequence voltage inside the converter is the difference in the power generated in the cluster and the per phase power absorbed by the grid

$$P_{az} = \mathrm{Re}\{\boldsymbol{V_z I_a^*}\} = V_z I_g \cos(\alpha+\gamma) = P_a - \frac{P_g}{3} = \frac{2P_a - P_b - P_c}{3} \tag{3}$$

$$P_{bz} = \mathrm{Re}\{\mathrm{Re}\{\boldsymbol{V_z I_b^*}\}\} = V_z I_g \cos\left(\alpha+\gamma+\frac{2\pi}{3}\right) = P_b - \frac{P_g}{3} = \frac{2P_b - P_a - P_c}{3}. \tag{4}$$

Similarly,

$$P_{cz} = P_c - \frac{P_g}{3} = \frac{2P_c - P_b - P_a}{3}. \tag{5}$$

Here, α is an angle between V_{an} and V_z, γ denotes a power factor angle between grid current $(I_g = I_a = I_b = I_c)$, and grid voltage $(V_g = V_{\mathrm{an}} = V_{bn} = V_{cn})$, and I_g is per phase grid current, which is written as

$$I_g = \frac{P_g}{3V_g \cos\gamma}. \tag{6}$$

From (4), one obtains

$$-\frac{V_z I_g \cos(\alpha+\gamma)}{2} - \frac{\sqrt{3}V_z I_g \sin(\alpha+\gamma)}{2} = \frac{2P_b - P_a - P_c}{3}. \tag{7}$$

Substituting (3) into (7), one gets

$$V_z I_g \sin(\alpha+\gamma) = \frac{P_c - P_b}{\sqrt{3}}. \tag{8}$$

It can be observed that (8) denotes the reactive power supplied by the zero-sequence voltage for phase a. It can be written as

$$Q_{az} = \mathrm{Img}\{\boldsymbol{V_z I_a^*}\} = V_z I_g \sin(\alpha+\gamma) = \frac{P_c - P_b}{\sqrt{3}}. \tag{9}$$

A similar analysis is done for the other two phases

$$Q_{bz} = \mathrm{Img}\{\boldsymbol{V_z I_b^*}\} = V_z I_g \sin\left(\alpha+\gamma+\frac{2\pi}{3}\right) = \frac{P_a - P_c}{\sqrt{3}} \tag{10}$$

$$Q_{cz} = \mathrm{Img}\{\boldsymbol{V_z I_c^*}\} = V_z I_g \sin\left(\alpha+\gamma-\frac{2\pi}{3}\right) = \frac{P_b - P_a}{\sqrt{3}}. \tag{11}$$

From (3)–(5) and (9)–(11), it can be seen that $P_{az} + P_{bz} + P_{cz} = 0$ and $Q_{az} + Q_{bz} + Q_{cz} = 0$. Thus, the sum of active and reactive power generated by the zero-sequence voltage with per phase grid current is zero. It means that V_z does not provide any extra power to the grid. The function of the zero-sequence voltage is, therefore, to circulate excess power from one phase to another.

By solving (3) and (8), the magnitude of zero-sequence voltage and angle α is given as

$$V_z = \frac{2V_g \cos\gamma}{P_g}\sqrt{P_a^2 + P_b^2 + P_c^2 - P_aP_b - P_bP_c - P_cP_a} \tag{12}$$

$$\alpha = \begin{cases} -\gamma + \tan^{-1}\left(\frac{\sqrt{3}(P_c-P_b)}{2P_a-P_b-P_c}\right) & \text{for } Q_g > 0 \\ \gamma + \tan^{-1}\left(\frac{\sqrt{3}(P_c-P_b)}{2P_a-P_b-P_c}\right) & \text{for } Q_g < 0 \\ \tan^{-1}\left(\frac{\sqrt{3}(P_c-P_b)}{2P_a-P_b-P_c}\right) & \text{for } Q_g = 0 \end{cases}. \tag{13}$$

During fault condition, $P_a \neq P_b \neq P_c$, a generalized expression of V_z is depicted in (12). For solar PV fed converter, γ can be varied between $-\pi/2$ and $\pi/2$. For $-\pi/2 < \gamma < 0$, the reactive power is absorbed by the grid (lagging power factor), and for $0 < \gamma < \pi/2$, the reactive power is supplied by the grid (leading power factor). For $\cos\gamma = 1$, the expression of V_z has been reported in [25].

III. Effect of Available DC-Link Voltage on Active and Reactive Power Capacity of Converter

In addition to V_z, the required voltage magnitude of some clusters will increase while for some other it will decrease. It might be possible that one of the required cluster voltages exceeds the available cumulative dc-link voltage after bypassing the faulty cells [6]. As a result, the converter will operate into the overmodulation region which is not desirable because of the generation of low-frequency harmonics. The required cluster voltage, therefore, must be less than its available dc-link voltage. The expression of required cluster voltages during fault condition is derived below.

The required phase cluster voltages under fault condition are written as

$$\boldsymbol{V_{ao}} = \boldsymbol{V_{an}} + j\omega L_f \boldsymbol{I_a} + \boldsymbol{V_z} = V_g \angle 0 + j\omega L_f I_g \angle -\gamma + V_z \angle \alpha \tag{14}$$

$$\boldsymbol{V_{bo}} = \boldsymbol{V_{bn}} + j\omega L_f \boldsymbol{I_b} + \boldsymbol{V_z} = V_g \angle -\frac{2\pi}{3} + j\omega L_f I_g \angle \left(-\frac{2\pi}{3} - \gamma\right) + V_z \angle \alpha \tag{15}$$

$$\boldsymbol{V_{co}} = \boldsymbol{V_{cn}} + j\omega L_f \boldsymbol{I_c} + \boldsymbol{V_z}$$
$$= V_g \angle \frac{2\pi}{3} + j\omega L_f I_g \angle \left(\frac{2\pi}{3} - \gamma\right) + V_z \angle \alpha. \quad (16)$$

From Fig. (2), an apparent power supplied by the converter is given as

$$\boldsymbol{S_a} = \boldsymbol{V_{ao}} \boldsymbol{I_a^*} = P_a + jQ_a$$
$$= \frac{P_g}{3} + j\frac{Q_g}{3} + P_{az} + jQ_{az} + jI_g^2 \omega L_f \quad (17)$$
$$\boldsymbol{S_b} = \boldsymbol{V_{bo}} \boldsymbol{I_b^*} = P_b + jQ_b$$
$$= \frac{P_g}{3} + j\frac{Q_g}{3} + P_{bz} + jQ_{bz} + jI_g^2 \omega L_f \quad (18)$$
$$\boldsymbol{S_c} = \boldsymbol{V_{co}} \boldsymbol{I_c^*} = P_c + jQ_c$$
$$= \frac{P_g}{3} + j\frac{Q_g}{3} + P_{cz} + jQ_{cz} + jI_g^2 \omega L_f. \quad (19)$$

From (17), the required cluster voltage for phase a can be written as

$$V_{ao} = \left|\frac{\boldsymbol{S_a}}{\boldsymbol{I_a^*}}\right| = \frac{\sqrt{P_a^2 + \left(\frac{Q_g}{3} + Q_{az} + I_g^2 \omega L_f\right)^2}}{I_g}. \quad (20)$$

Substituting the value of I_g from (6) to (20), one obtains

$$V_{ao} = \left|\frac{\boldsymbol{S_a}}{\boldsymbol{I_a^*}}\right|$$
$$= \frac{3V_g \cos\gamma \sqrt{P_a^2 + \left(\frac{Q_g}{3} + Q_{az} + \left(\frac{P_g}{3V_g \cos\gamma}\right)^2 \omega L_f\right)^2}}{P_g}. \quad (21)$$

Similarly, the required cluster voltage for phase b and c are obtained as

$$V_{bo} = \left|\frac{\boldsymbol{S_b}}{\boldsymbol{I_b^*}}\right|$$
$$= \frac{3V_g \cos\gamma \sqrt{P_b^2 + \left(\frac{Q_g}{3} + Q_{bz} + \left(\frac{P_g}{3V_g \cos\gamma}\right)^2 \omega L_f\right)^2}}{P_g} \quad (22)$$

$$V_{co} = \left|\frac{\boldsymbol{S_c}}{\boldsymbol{I_c^*}}\right|$$
$$= \frac{3V_g \cos\gamma \sqrt{P_c^2 + \left(\frac{Q_g}{3} + Q_{cz} + \left(\frac{P_g}{3V_g \cos\gamma}\right)^2 \omega L_f\right)^2}}{P_g}. \quad (23)$$

Few observations are made from (21)–(23). Among all the parameters, the magnitude of grid voltage (V_g) and grid interface inductor (L_f) are fixed, and remaining parameters vary with active power generated from the clusters $(P_a,\ P_b$ and $P_c)$ and reactive power (Q_g) exchange with the grid. For example, the power factor $(\cos\gamma)$ varies with the active (P_g) and reactive power exchange with the grid. The active power generated from the clusters is dependent on healthy cells available in the clusters. The zero-sequence reactive powers $(Q_{az},\ Q_{bz},$ and $Q_{cz})$ are dependent on the power unbalance among the clusters.

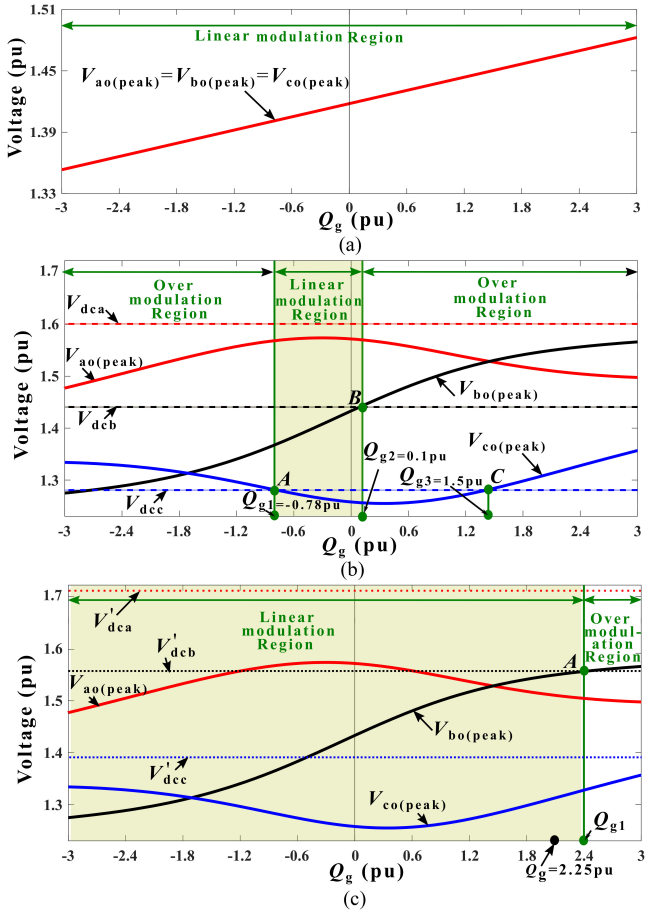

Fig. 4. Variation of peak value of cluster voltages with reactive power exchange with the grid. (a) Prefault. (b) Postfault n_a =0, $n_b = 1$, and $n_c = 2$. (c) Extended linear modulation region with fault $n_a = 0$, $n_b = 1$, and $n_c = 2$.

The required dc-link voltage should be such that the required magnitude of cluster voltages can be realized to prevent over modulation. The required dc-link voltage during prefault and postfault condition is explained in Section III-A.

A. *Prefault Condition*

In prefault condition, the active power produced from the clusters $(P_a = P_b = P_c)$ are equal. Therefore, in (21)–(23), the required cluster voltages vary with the change in Q_g. As the demand for the reactive power increases, therefore, the required dc-link voltage increases as shown in Fig. 4(a). To prevent over modulation, the required cumulative dc-link voltage must be more than required cluster voltage, i.e.,

$$V_{\mathrm{dc}i} = nk \geq \frac{S_f}{m} V_{io(\mathrm{peak})} \quad \forall i \in (a, b, c) \quad (24)$$

where $V_{io(\mathrm{peak})}$ is equal to $\sqrt{2}$ times the rms value shown in (21)–(23) and m is the modulation index and S_f is the safety

factor of each device. Here, k is the required dc-link voltage of each cell of the clusters, i.e.,

$$V_{\mathrm{dc}ij} = k \geq \frac{V_{\mathrm{dc}i}}{n} \quad \forall i \in (a,b,c), \quad j \in (1,\ldots,n). \tag{25}$$

The converter during prefault condition will operate steadily with the value of k given in (25) for certain active and reactive power exchange with the grid. The required value of k to prevent overmodulation is shown with an example.

It is assumed that during prefault condition, total number of cells is $n = 10$ and active power generated from each cell is 0.1 per unit (p.u.) and grid voltage $V_g = 1$ p.u.. The required cluster voltage are $V_{ao} = V_{bo} = V_{co} = 1.032$ p.u. from (21)–(23) assuming that $Q_g = 2.25$ p.u., $L_f = 0.05$ p.u., and $P_a = P_b = P_c = 1$ p.u. From (9)–(11), the zero-sequence reactive power are $Q_{az} = Q_{bz} = Q_{cz} = 0$ p.u. Therefore, the required peak value of cluster voltages are $V_{ao(\mathrm{peak})} = V_{bo(\mathrm{peak})} = V_{co(\mathrm{peak})} = \sqrt{2} * 1.032 = 1.46$ p.u. The cumulative dc-link voltage is calculated from (24) by taking $m = 1$ and $S_f = 1.1$. Hence, the cumulative dc-link voltage of the clusters is 1.6 p.u., and individual dc-link voltage of each cell is calculated from (25) as $k = 1.6/10 = 0.16$ p.u.

B. Postfault Condition

During postfault condition some cells are bypassed. Hence, the active power supply to the grid is reduced. The reactive power exchange with the grid is likely to change because the converter produces different magnitudes of cluster voltages. Hence, the required dc-link voltage of the cluster will change. The required dc-link voltage after bypassing faulty cells is written as

$$V_{\mathrm{dc}i} = (n - n_i)k \geq \frac{S_f(n-n_i)}{m} \times \max\left(\frac{V_{ao(\mathrm{peak})}}{n-n_a}, \frac{V_{bo(\mathrm{peak})}}{n-n_b}, \frac{V_{co(\mathrm{peak})}}{n-n_c}\right) \quad \forall i \in (a,b,c). \tag{26}$$

From (26), required dc-link voltage of each cell (k) is obtained as

$$V_{\mathrm{dc}ij} = k \geq \frac{S_f}{m} \max\left(\frac{V_{ao(\mathrm{peak})}}{n-n_a}, \frac{V_{bo(\mathrm{peak})}}{n-n_b}, \frac{V_{co(\mathrm{peak})}}{n-n_c}\right) \quad \forall i \in (a,b,c) \text{ and } j \in (1,\ldots,n). \tag{27}$$

Now, the required value of cumulative dc-link voltages is shown with an example during a postfault condition.

It is assumed that some faults have occurred in the clusters such that $n_a = 0, n_b = 1$, and $n_c = 2$. The active power supplied to the grid will reduce due to bypass of the faulty cells. Therefore, from (1), the cluster powers are $P_a = 1$ p.u., $P_b = 0.9$, and $P_c = 0.8$ p.u. From (9)–(11), the zero-sequence reactive power are $Q_{az} = -0.057$ p.u., $Q_{bz} = 0.115$ p.u., and $Q_{cz} = -0.057$. Hence, all three cluster voltages become unequal [from (21)–(23)]. Their peak values are $V_{ao(\mathrm{peak})} = 1.50$ p.u., $V_{bo(\mathrm{peak})} = 1.55$ p.u., and $V_{co(\mathrm{peak})} = 1.32$ p.u. for $Q_g = 2.25$ p.u. The cumulative dc-link voltages are calculated from (26) by putting $n = 10$, $n_a = 0$, $n_b = 1$, $n_c = 2$, $m = 1$, and $S_f = 1.1$. Hence,

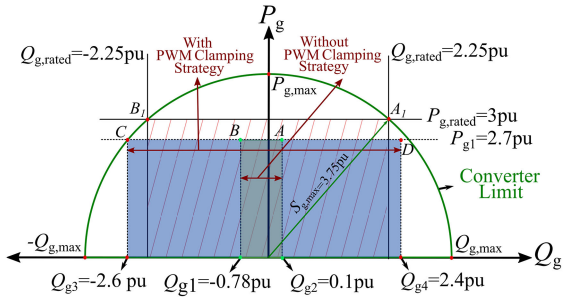

Fig. 5. PQ diagram of the converter.

$V_{\mathrm{dc}a} = 1.72$ p.u., $V_{\mathrm{dc}b} = 1.54$, and $V_{\mathrm{dc}c} = 1.37$ p.u. The required dc-link voltage is calculated from (27) as $k = 0.172$ p.u.

From both the examples, it is found out that the required dc-link voltage of each cell is increased from $k = 0.16$ p.u. to $k = 0.172$ p.u. for supplying $Q_g = 2.25$ p.u. to the grid.

If the dc-link voltage of cells is maintained the same in both the prefault and postfault condition ($k = 0.16$ p.u.) then the amount of reactive power exchange with the grid is limited.

For $k = 0.16$ p.u., the cumulative dc-link voltage of clusters are $V_{\mathrm{dc}a} = 0.16 * 10 = 1.6$ p.u., $V_{\mathrm{dc}b} = 0.16 * 9 = 1.44$, and $V_{\mathrm{dc}c} = 0.16 * 8 = 1.28$ p.u.

The converter supplies reactive power between $Q_{g1} = -0.78$ p.u. and $Q_{g2} = 0.1$ p.u. to the grid because the cluster voltages are within their available cumulative dc-link voltage. The region shown by two-line passing through A and B in Fig. 4(b) is the converter operating region. If Q_g is between A and B, the converter operates in linear modulation region. If Q_g is outside the shaded region, the converter operates in overmodulation region that results in unbalanced and distorted grid currents.

This narrow region can be extended by using a novel PWM clamping strategy which is explained in Section IV. Using this strategy, the linear modulation region is increased. Therefore, the reactive power exchanging capability of the converter is extended. In Fig. 4(c), it can be seen that the converter can supply reactive power up to 2.4 p.u. using the novel PWM technique which in Fig. 4(b) was only 0.1 p.u.

The operating region in the PQ diagram of the converter during prefault and postfault is shown in Fig. 5.

The maximum apparent power exchanged with the grid can be written as

$$S_{g,\max} = \sqrt{P_g^2 + Q_g^2}. \tag{28}$$

In the prefault condition, the operating region in the PQ diagram of the converter is between point A_1 and B_1, where the converter supplies $P_{\mathrm{g,rated}} = 3$ p.u. active power and exchanges $Q_{g,\mathrm{rated}} = \pm 2.25$ p.u. reactive power with the grid. In the postfault condition, the operating region in PQ diagram is reduced which is shown between point A and B. In this region, the converter supplies $P_{g1} = 2.7$ p.u. and can exchange limited reactive power between $Q_{g1} = -0.78$ p.u. and $Q_{g2} = 0.1$ p.u. due to available dc-link voltage of the clusters. The operating region between points A and B can be extended to points C

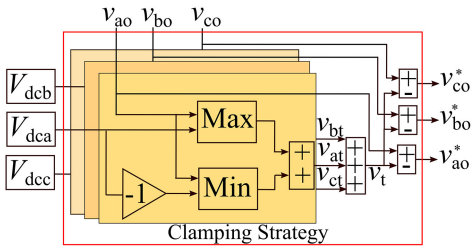

Fig. 6. Block diagram of PWM clamping strategy.

and D using a novel PWM clamping strategy, to be explained in Section IV. Now, the converter can exchange reactive power between $Q_{g3} = -2.6$ p.u. and $Q_{g4} = 2.4$ p.u.

IV. Novel PWM Strategy

In this section, a novel PWM clamping strategy is used so that the reactive power capability of the converter is extended.

As seen in Fig. 4(b), the magnitude of some of the cluster voltages increases when more reactive power is supplied to the grid in a postfault condition. Thus, there is a possibility of converter working in the overmodulation region. On the other hand, with limited available cumulative dc-link voltage during the postfault operation, the converter exchanges limited reactive power with the grid to avoid overmodulation. The overmodulation can be suppressed and reactive power exchange can be extended by increasing the linear modulation region through a novel PWM clamping strategy. This strategy restricts the reference voltages within the available dc-link voltage.

The overmodulation of CHB converter is confirmed if $|v_{io}| > \mathrm{V}_{dci}$. To prevent over modulation, the reference voltage is modified according to the clamping strategy (see Fig. 6).

In each phase, the maximum and minimum instantaneous signals are extracted from the reference v_{io} and cumulative dc-link voltage V_{dci}; addition of these two signals, v_{it} is obtained as

$$v_{it} = \max(v_{io}, V_{\mathrm{dci}}) + \min(v_{io}, -V_{\mathrm{dci}}) \quad \forall i \in \{a, b, c\}. \tag{29}$$

The common mode signal v_t is computed as

$$v_t = \sum_{i=a}^{i=c} v_{it}. \tag{30}$$

This signal is subtracted from the reference v_{io} in order to get the modified PWM reference $v_{io}*$, i.e.,

$$v^*_{io} = v_{io} - v_t. \tag{31}$$

Assume, for the fault condition $n_a = 0$, $n_b = 1$, and $n_c = 2$, the converter supplies $P_g = 2.7$ p.u. and $Q_g = 2.25$ p.u. to the grid. The available dc-link voltages are $V_{\mathrm{dca}} = 10k = 1.6$ p.u., $V_{\mathrm{dcb}} = 9k = 1.44$, and $V_{\mathrm{dcc}} = 8k = 1.28$ p.u., where $k = 0.16$ p.u. From (21)–(23), the reference voltage of the converter (v_{io}) are obtained as shown in Fig. 7(a). It can be seen that v_{bn} and v_{cn} cross their available dc-link voltages of $9k$ and $8k$, respectively. This leads to the overmodulation operation causing unwanted harmonics to appear at converter output voltages. In

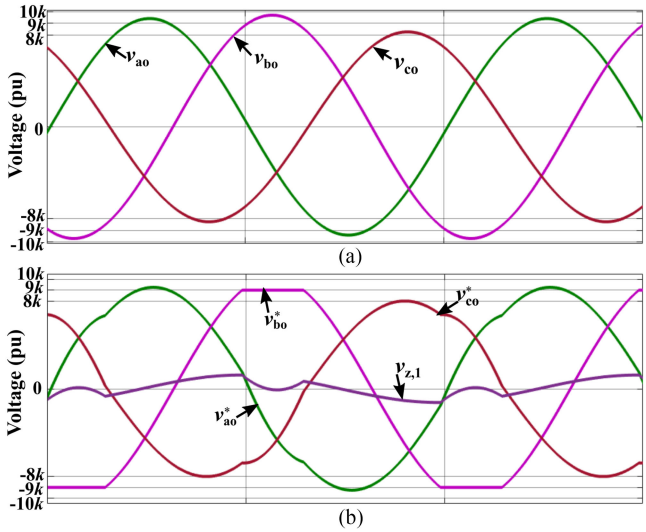

Fig. 7. Waveforms for $n_a = 0$, $n_b = 1$, and $n_c = 2$. (a) Reference voltage for converter (v_{io}). (b) Waveforms using proposed control method: modified reference $(v_{io}*)$ and modified zero-sequence voltage $(v_{z,1})$.

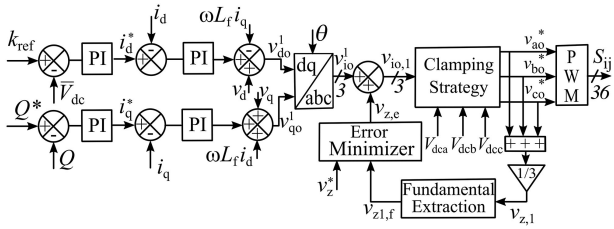

Fig. 8. Control diagram of the grid connected CHB converter during fault with exact zero-sequence voltage tracking.

the clamping strategy, the waveform part in v_{bo} above $9k$ p.u. and the waveform part in v_{co} above $8k$ p.u. are clamped.

To insert the exact magnitude and phase of v_z, a control scheme is proposed in Fig. 8. The main focus of this control strategy is to insert v_z according to (12) and (13), given as v^*_z. Note that v^*_z from (12) and (13) consists of only fundamental frequency voltage, however, it may be possible to add additional harmonics in v_z [7], [21], [22]. In the control scheme (see Fig. 8), a clamping block is added in conventional control of CHB converter [27]. First $v_{z,1}$ is calculated as

$$v_{z,1} = (v^*_{ao} + v^*_{bo} + v^*_{co})/3. \tag{32}$$

Here, $v_{z,1}$ contains fundamental and higher harmonic voltages. The fundamental voltage $(v_{zf,1})$ is extracted from $v_{z,1}$ and given to the error minimizer block with reference v^*_z. The output signal of error minimizer block is added with the reference voltages to generate three signals for clamping block. The modified reference voltages (v^*_{io}) shown in Fig. 7(b) are obtained from the clamping block which are equal and lower than their dc-link voltages. The zero-sequence voltage $(v_{z,1})$ needed for clamping is shown in Fig. 7(b) that has same fundamental magnitude and phase given in (12) and (13).

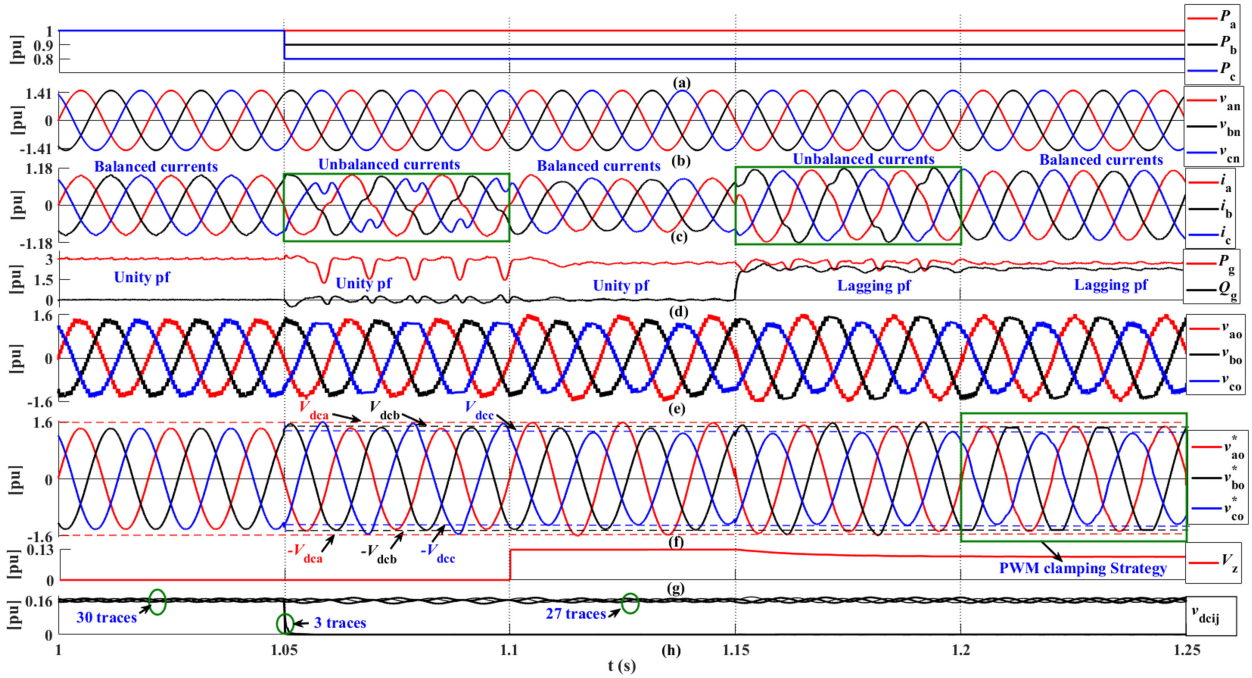

Fig. 9. Simulation results for $n_a = 0$, $n_b = 1$, and $n_c = 2$. (a) Active power of each cluster. (b) Grid voltages. (c) Grid currents. (d) Three-phase active and reactive power. (e) Cluster voltages. (f) Reference voltage for the clusters. (g) Zero-sequence voltage. (h) DC-link voltage of each cluster.

TABLE I
SIMULATION AND EXPERIMENTAL PARAMETERS

Description	Parameter	Simulation Values	Experimental Values
Rated active power	P_g	10 MW (3 pu)	1 kW
Rated reactive power	Q_g	7.5 MVAR (2.25 pu)	0.75 kVAR
Line to line Grid voltage	$V_{l\text{-}l}$	6.6 kV (1.732 pu)	150 V
No of cells in a cluster	n	10	3
DC link voltage of a cluster	V_{dcj}	6.1 kV (1.6 pu)	144 V
Each cluster active power	P_i	3.33 MW (1 pu)	333 W
Phase grid voltage	V_g	3810.51 (1 pu)	86.60 V
Switching frequency of a device	f_{sw}	1.6 kHz	1.6 kHz
Inductor	L_f	0.05 pu	0.05 pu

V. SIMULATION RESULTS

The operation of solar PV fed CHB converter during prefault and postfault conditions is presented through MATLAB/Simulink software. In the simulation, solar PV with dc–dc converter is considered as a controllable current source [7]. The simulation parameters are given in Table I.

Fig. 9 explains the operation of solar PV fed CHB converter during prefault and postfault conditions. From $t = 1$ s to $t = 1.05$ s, the converter operates without any fault. The active power generated from the clusters are $P_a = P_b = P_c = 1$ p.u. Therefore, the converter output voltages and currents are balanced as shown in Fig. 9(e) and (c), respectively.

Now, faults have occurred in the clusters such that $n_a = 0$, $n_b = 1$, and $n_c = 2$. It means that one cell in phase "b" and two cells in phase "c" are faulty, therefore, they are bypassed. The active power generation from the clusters are now $P_a = 1$ p.u., $P_b = 0.9$ p.u., and $P_c = 0.8$ according to (1) as shown in Fig. 9(a).

From $t = 1.05$ s to $t = 1.1$ s, after bypassing the faulty cells, the reference voltages of the cluster get unbalanced, and some of the reference voltages exceed their dc-link voltage as shown in Fig. 9(f). Therefore, the converter injects unbalanced currents into the grid [see Fig. 9(c)].

From $t = 1.1$ s to $t = 1.15$ s, the zero-sequence voltage is injected according to (12) [see Fig. 9(g)]. The reference voltages now come within their dc-link voltage [see Fig. 9(f)]. Now, the grid currents are balanced [see Fig. 9(c)]. In this condition, the converter supply $P_g = 2.7$ p.u. in the grid as shown in Fig. 9(d).

From $t = 1.15$ s to 1.25 s, the converter supplies both active and reactive power ($P_g = 2.7$ p.u. and $Q_g = 2.25$ p.u.) to the grid as shown in Fig. 9(d). Because of the supply of reactive power, from $t = 1.15$ s to $t = 1.2$ s, the reference voltages exceed their dc-link voltage. Therefore, the grid currents again become unbalanced.

Now, the proposed PWM clamping strategy is used from $t = 1.2$ s to $t = 1.25$ s. The reference voltages are restricted within their dc-link voltage. Therefore, the grid currents become balanced [see Fig. 9(c)]

VI. EXPERIMENTAL RESULTS

A laboratory setup is used to verify simulation results of the fault-tolerant operation of the three-phase grid-connected seven-level CHB converter. In the prefault condition, the

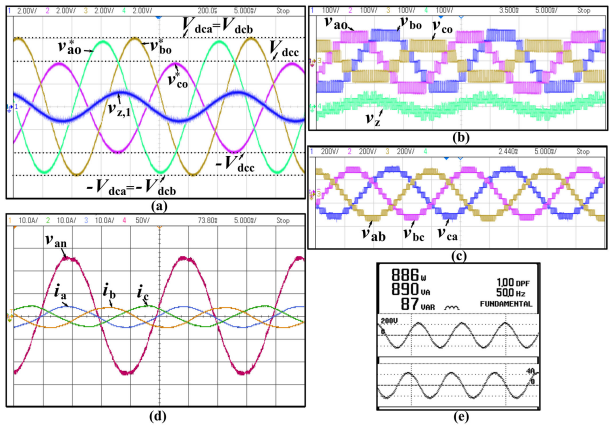

Fig. 10. Waveforms for $n_a = 0$, $n_b = 0$, and $n_c = 1$ with injection of reactive power without PWM clamping strategy. (a) Reference voltages and zero-sequence voltage. (b) Cluster voltages (100 V/div) and zero-sequence voltage (100 V/div). (c) Line voltages of the converter (200 V/div). (d) Three-phase grid currents (10 A/div) and grid voltage (50 V/div). (e) Active and reactive power injected into the grid.

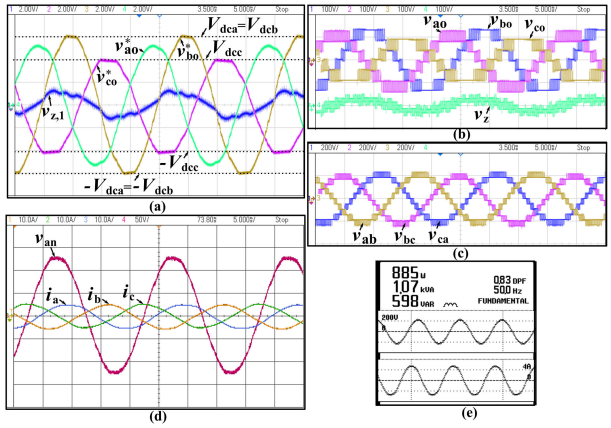

Fig. 11. Waveforms for $n_a = 0$, $n_b = 0$, and $n_c = 1$ with injection of reactive power without PWM clamping strategy. (a) Reference voltages and zero-sequence voltage. (b) Cluster voltages (100 V/div) and zero-sequence voltage (100 V/div). (c) Line voltages of the converter (200 V/div). (d) Three-phase grid currents (10 A/div) and grid voltage (50 V/div). (e) Active and reactive power injected into the grid.

experimental parameters are given in Table I. The PWM signals for the CHB multilevel converter are produced from the combination of the TMS320F28335 Delfino microcontroller and Max 10 field-programmable gate array (FPGA) controller.

To validate the concept, the experimental results shows for $n_a = n_b = 0$ and $n_c = 1$. In Fig. 10, the converter is supplying active power $P_g = 888$ W and reactive power $Q_g = 90$ VAR to the grid. In this condition, A zero-sequence voltage [from (21)–(23)] is injected to obtained required cluster voltage references as shown in Fig. 10(a). It can be seen that the peak of cluster voltage references is within their dc-link voltage. The unbalanced cluster voltages and zero-sequence voltage are shown in Fig. 10(b). The line voltage obtained from the converter is balanced [see Fig. 10(c)]. The grid currents are balanced, and somewhat lagging to the grid voltage in Fig. 10(d). Fig. 10(e) shows active and reactive power injected into the grid.

Now, the converter is supplying active power $P_g = 888$ W and reactive power $Q_g = 600$ VAR to the grid. Some of the required cluster voltages exceed their dc-link voltage. So the PWM clamping strategy is used. It can be seen in Fig. 11(a) that the required cluster voltage is limited to their dc-link voltage and zero-sequence voltage is also shown. The output voltage of the clusters and zero-sequence voltage are shown in Fig. 11(b). In this condition, the line voltage still balanced as shown in Fig. 11(c). The grid currents are still balanced and lag to the grid voltage as shown in Fig. 11(d).

VII. Conclusion

The grid-tied CHB multilevel converter for the solar PV system has been discussed during cell fault in the cluster. The zero-sequence voltage has been analyzed and derived when the converter exchanges certain active power and reactive power with the grid. The mathematical expression of the required dc-link voltage to prevent overmodulation region has been derived. It is shown through simulation and experimental results that the zero-sequence voltage can extend the reactive power capability of the converter as well as balance the unbalanced voltages. A novel PWM clamping strategy is also proposed and verified that helps to prevent overmodulation operation of the converter.

References

[1] J. Sastry, P. Bakas, H. Kim, L. Wang, and A. Marinopoulos, "Evaluation of cascaded H-bridge inverter for utility-scale photovoltaic systems," *Renew. Energy*, vol. 69, pp. 208–218, Sep. 2014.

[2] E. Romero-Cadaval, B. Francois, M. Malinowski, and Q. Zhong, "Grid-connected photovoltaic plants: An alternative energy source, replacing conventional sources," *IEEE Ind. Electron. Mag.*, vol. 9, no. 1, pp. 18–32, Mar. 2015.

[3] H. D. Tafti, A. I. Maswood, G. Konstantinou, C. D. Townsend, P. Acuna, and J. Pou, "Flexible control of photovoltaic grid-connected cascaded H-bridge converters during unbalanced voltage sags," *IEEE Trans. Ind. Electron.*, vol. 65, no. 8, pp. 6229–6238, Aug. 2018.

[4] J. Chavarria, D. Biel, F. Guinjoan, C. Meza, and J. J. Negroni, "Energy-balance control of PV cascaded multilevel grid-connected inverters under level-shifted and phase-shifted PWMs," *IEEE Trans. Ind. Electron.*, vol. 60, no. 1, pp. 98–111, Jan. 2013.

[5] M. Malinowski, K. Gopakumar, J. Rodriguez, and M. A. Perez, "A survey on cascaded multilevel inverters," *IEEE Trans. Ind. Electron.*, vol. 57, no. 7, pp. 2197–2206, Jul. 2010.

[6] H. Akagi, "Classification, terminology, and application of the modular multilevel cascade converter (MMCC)," *IEEE Trans. Power Electron.*, vol. 26, no. 11, pp. 3119–3130, Nov. 2011.

[7] P. Sochor and H. Akagi, "Theoretical comparison in Energy-balancing capability between star- and delta-configured modular multilevel cascade inverters for utility-scale photovoltaic systems," *IEEE Trans. Power Electron.*, vol. 31, no. 3, pp. 1980–1992, Mar. 2016.

[8] M. R. Islam, Y. Guo, and J. Zhu, "A high-frequency link multilevel cascaded medium-voltage converter for direct grid integration of renewable energy systems," *IEEE Trans. Power Electron.*, vol. 29, no. 8, pp. 4167–4182, Aug. 2014.

[9] S. Essakiappan, H. S. Krishnamoorthy, P. Enjeti, R. S. Balog, and S. Ahmed, "Multilevel medium-frequency link inverter for utility scale photovoltaic integration," *IEEE Trans. Power Electron.*, vol. 30, no. 7, pp. 3674–3684, Jul. 2015.

[10] P. Lezana, J. Pou, T. A. Meynard, J. Rodriguez, S. Ceballos, and F. Richardeau, "Survey on fault operation on multilevel inverters," *IEEE Trans. Ind. Electron.*, vol. 57, no. 7, pp. 2207–2218, Jul. 2010.

[11] W. Zhang, D. Xu, P. N. Enjeti, H. Li, J. T. Hawke, and H. S. Krishnamoorthy, "Survey on fault-tolerant techniques for power electronic converters," *IEEE Trans. Power Electron.*, vol. 29, no. 12, pp. 6319–6331, Dec. 2014.

[12] J. Rodriguez, P. W. Hammond, J. Pontt, R. Musalem, P. Lezana, and M. J. Escobar, "Operation of a medium-voltage drive under faulty conditions," *IEEE Trans. Ind. Electron.*, vol. 52, no. 4, pp. 1080–1085, Aug. 2005.
[13] P. Lezana and G. Ortiz, "Extended operation of cascade multicell converters under fault condition," *IEEE Trans. Ind. Electron.*, vol. 56, no. 7, pp. 2697–2703, Jul. 2009.
[14] F. Carnielutti, H. Pinheiro, and C. Rech, "Generalized carrier-based modulation strategy for cascaded multilevel converters operating under fault conditions," *IEEE Trans. Ind. Electron.*, vol. 59, no. 2, pp. 679–689, Feb. 2012.
[15] S. Ouni *et al.*, "Improvement of post-fault performance of a cascaded H-bridge multilevel inverter," *IEEE Trans. Ind. Electron.*, vol. 64, no. 4, pp. 2779–2788, Apr. 2017.
[16] W. Song and A. Q. Huang, "Fault-tolerant design and control strategy for cascaded H-bridge multilevel converter-based STATCOM," *IEEE Trans. Ind. Electron.*, vol. 57, no. 8, pp. 2700–2708, Aug. 2010.
[17] Y. Neyshabouri and H. Iman-Eini, "A new fault-tolerant strategy for a cascaded H-bridge based STATCOM," *IEEE Trans. Ind. Electron.*, vol. 65, no. 8, pp. 6436–6445, Aug. 2018.
[18] H. Salimian and H. Iman-Eini, "Fault-tolerant operation of three-phase cascaded H-bridge converters using an auxiliary module," *IEEE Trans. Ind. Electron.*, vol. 64, no. 2, pp. 1018–1027, Feb. 2017.
[19] L. Maharjan, T. Yamagishi, H. Akagi, and J. Asakura, "Fault-tolerant operation of a battery-energy-storage system based on a multilevel cascade PWM converter with star configuration," *IEEE Trans. Power Electron.*, vol. 25, no. 9, pp. 2386–2396, Sep. 2010.
[20] B. Xiao, L. Hang, J. Mei, C. Riley, L. M. Tolbert, and B. Ozpineci, "Modular cascaded H-bridge multilevel PV inverter with distributed MPPT for grid-connected applications," *IEEE Trans. Ind. Appl.*, vol. 51, no. 2, pp. 1722–1731, Mar./Apr. 2015.
[21] Y. Yu, G. Konstantinou, B. Hredzak, and V. G. Agelidis, "Power balance of cascaded H-bridge multilevel converters for large-scale photovoltaic integration," *IEEE Trans. Power Electron.*, vol. 31, no. 1, pp. 292–303, Jan. 2016.
[22] Y. Yu, G. Konstantinou, C. D. Townsend, and V. G. Agelidis, "Comparison of zero-sequence injection methods in cascaded H-bridge multilevel converters for large-scale photovoltaic integration," *IET Renew. Power Gener.*, vol. 11, no. 5, pp. 603–613, April 2017.
[23] L. Liu, H. Li, Y. Xue, and W. Liu, "Reactive power compensation and optimization strategy for grid-interactive cascaded photovoltaic systems," *IEEE Trans. Power Electron.*, vol. 30, no. 1, pp. 188–202, Jan. 2015.
[24] L. Liu, H. Li, Y. Xue, and W. Liu, "Decoupled active and reactive power control for large-scale grid-connected photovoltaic systems using cascaded modular multilevel converters," *IEEE Trans. Power Electron.*, vol. 30, no. 1, pp. 176–187, Jan. 2015.
[25] Y. Yu, G. Konstantinou, B. Hredzak, and V. G. Agelidis, "Operation of cascaded H-bridge multilevel converters for large-scale photovoltaic power plants under bridge failures," *IEEE Trans. Ind. Electron.*, vol. 62, no. 11, pp. 7228–7236, Nov. 2015.
[26] J. Lamb, B. Mirafzal, and F. Blaabjerg, "PWM common mode reference generation for maximizing the linear modulation region of CHB converters in islanded microgrids," *IEEE Trans. Ind. Electron.*, vol. 65, no. 7, pp. 5250–5259, Jul. 2018.
[27] H. Akagi, S. Inoue, and T. Yoshii, "Control and performance of a transformerless cascade PWM STATCOM with star configuration," *IEEE Trans. Ind. Appl.*, vol. 43, no. 4, pp. 1041–1049, Jul./Aug. 2007.
[28] *IEEE Standard for Interconnecting Distributed Resources With Electric Power Systems*, IEEE Standard 1547, 2003.

Rahul Sharma (S'18) was born in Jaipur, Rajasthan, India. He received the B.E. degree in electrical engineering from the College of Technology and Engineering, Udaipur, Rajasthan, India, in 2014, and the M.Tech. degree in power electronics and drives from the Motilal Nehru National Institute of Technology, Allahabad, India, in 2016. He is currently working toward the Ph.D. degree with the Department of Electrical Engineering, Indian Institute of Technology, Delhi, New Delhi, India.

He was the recipient of Gold Medal in power electronics and drives specialization in M.Tech degree. His areas of research interests include high power electronic converters, power quality, HVdc, and renewable energy systems.

Anandarup Das (S'07–M'10) received the Ph.D. degree in power electronics from the Center for Electronics Design and Technology, Indian Institute of Science, Bangalore, India, in 2010.

From 2010 to 2012, he was a Postdoctoral Researcher with the Norwegian University of Science and Technology, Trondheim, Norway. From 2012 to 2014, he worked in Siemens Power Electronics Centre (R&D) under Oil and Gas Division, Siemens, Norway as a Senior Development Engineer. He is currently an Assistant Professor with the Department of Electrical Engineering, Indian Institute of Technology, Delhi, New Delhi, India. His current research interests include high power multilevel converters, pulsewidth modulation techniques, power quality, and motor drives for various applications in electrical industries.